Physics Letters B 816 (2021) 136226

Contents lists available at ScienceDirect

Physics Letters B

www.elsevier.com/locate/physletb

Shell inhibition on production of $N = 126$ isotones in multinucleon transfer reactions

Long Zhu

Sino-French Institute of Nuclear Engineering and Technology, Sun Yat-sen University, Zhuhai 519082, China

ARTICLE INFO

Article history:
Received 25 January 2021
Received in revised form 16 March 2021
Accepted 16 March 2021
Available online 19 March 2021
Editor: W. Haxton

Keywords:
Multinucleon transfer reactions
Relative shell inhibition
$N = 126$
Unfavorable combinations
Cross sections

ABSTRACT

The multinucleon transfer process is one promising approach to produce exotic nuclei around the last "waiting point" in the r-process. However, the reliable reaction combinations are still ambiguous so far. We quantitatively evaluate the relative shell inhibition on production cross sections for producing $N = 126$ isotones for the first time with definition of a relative shell inhibition factor. The results suggest that the combinations characterized by double closed shell structure are unfavorable for producing unknown $N = 126$ isotones. It is demonstrated that the reactions ^{136}Xe + ^{208}Pb and ^{136}Xe + ^{198}Pt are not the good candidates. By investigating the yield contributions in main evaporation channels, we find that for producing ^{200}W the effects of shell structure on production cross sections are mainly from de-excitation process. Also, the weak incident energy dependence of cross sections for producing $N = 126$ isotones is revealed with relevance between evaporation probabilities and excitation energy distributions of primary fragments.

1. Introduction

The astrophysical r-process is responsible for the synthesis of about half of nuclei beyond iron. Understanding the important features of the r-process requires the knowledge of nuclei far from the stability, especially the nuclei along the $N = 126$ shell closure, which is the last "waiting point" in the r-process [1]. Moreover, the properties of these nuclei, unknown so far, are necessary to explore the shell structures in the nuclei with large neutron excess [2].

How to produce neutron-rich isotopes (NRI) along $N = 126$? The approach of fragmentation has been extensively applied to produce neutron-rich heavy nuclei [3–5]. However, the cross section decreases strongly when extended to the unknown $N = 126$ isotones. As one alternative path, the multinucleon transfer (MNT) process presents rather broad mass and charge distributions of products, which results in the high possibilities for producing exotic isotopes. In past decades, the mechanism of MNT process has been extensively investigated and great efforts have been made to produce new NRI [6–11]. Many combinations were performed experimentally [12–21] and several theoretical models have been applied to explore the mechanism of MNT process [22–41]. Nevertheless, no new isotopes with $N = 126$ have been observed. Because of low energies for target-like fragments (TLFs) produced in the MNT reactions, it is difficult to detect and identify them directly using spectrometer [42]. On the other side, the production yields are rather low. Therefore, in order to observe the unknown isotopes, apart from enhancing the efficiencies of the separation and detection system [18,43], the reaction combinations, which are at the heart of experiments, should be selected carefully.

The shell effects play an important role in MNT reactions and influence the nucleon diffusion process [44–50] as well as the excitation energy of the transfer products [44]. Based on the stabilizing effect of the closed neutron shells, the reaction ^{136}Xe + ^{208}Pb was proposed as one promising combination [51] and investigated extensively [15–17]. Recently, it was stated that the reaction ^{136}Xe + ^{198}Pt was more favorable because of larger transfer probabilities of neutrons compared to protons [12]. Also, several combinations with doubly magic partner, such as ^{58,64}Ni + ^{208}Pb [18–20], are widely investigated. However, in Ref. [52], it was observed that the magic shell characters unexpectedly suppress the intensity of nucleon diffusion. For the reactions with ^{208}Pb, the attraction of the shell closures ($Z = 82$ and $N = 126$) could suppress the probabilities of nucleon transfer and then lower the production cross sections of exotic nuclei. The shell effects on production cross sections have been investigated in many works. Nevertheless, it is still not clear how much influence of the shell effects on selection of optimal reaction systems could be.

In this work, within the framework of dinuclear system (DNS) model in combination with GEMINI++ code, we aim to qualitatively reveal the relative influence of shell structure on production

E-mail address: zhulong@mail.sysu.edu.cn.

https://doi.org/10.1016/j.physletb.2021.136226

of $N = 126$ isotones in deep inelastic collisions (DIC) and propose one perspective for selecting the favorable reaction systems. The DNS model has been successfully used in investigation of MNT reactions [22–28]. In Sec. 2, we briefly describe one extended version of DNS model (DNS-sysu) [10]. The results and discussion are presented in Sec. 3. Finally, we summarize the main results in Sec. 4.

2. Model

The master equation is one very general linear equation for the probability distribution. It is one suitable tool for describing DIC as the process of non-equilibrium state [53]. During the evolution in mass and charge asymmetry coordinates, the primary fragments can be obtained after a short contact time. In the DNS-sysu model, the fragment distribution probability can be calculated by solving the following master equation [10]:

$$\begin{aligned}
&\frac{dP(Z_1,N_1,\beta_2,J,t)}{dt}\\
&=\sum_{Z_1'} W_{Z_1,N_1,\beta_2;Z_1',N_1,\beta_2}(t)[d_{Z_1,N_1,\beta_2}P(Z_1',N_1,\beta_2,J,t)\\
&-d_{Z_1',N_1,\beta_2}P(Z_1,N_1,\beta_2,J,t)]\\
&+\sum_{N_1'} W_{Z_1,N_1,\beta_2;Z_1,N_1',\beta_2}(t)[d_{Z_1,N_1,\beta_2}P(Z_1,N_1',\beta_2,J,t)\\
&-d_{Z_1,N_1',\beta_2}P(Z_1,N_1,\beta_2,J,t)]\\
&+\sum_{\beta_2'} W_{Z_1,N_1,\beta_2;Z_1,N_1,\beta_2'}(t)[d_{Z_1,N_1,\beta_2}P(Z_1,N_1,\beta_2',J,t)\\
&-d_{Z_1,N_1,\beta_2'}P(Z_1,N_1,\beta_2,J,t)].
\end{aligned} \tag{1}$$

Here, $P(Z_1,N_1,\beta_2,J,t)$ is the distribution probability for the fragment 1 with proton number Z_1 and neutron number N_1 at time t. J is initial entrance angular momentum. β_2 is related to the dynamical deformation of the two collision partners [49]. $\delta\beta_2^1+\delta\beta_2^2 = 2\beta_2$, $C_1\delta\beta_2^1 = C_2\delta\beta_2^2$. $\delta\beta_2^1$ and $\delta\beta_2^2$ are dynamical quadrupole deformations of fragment 1 (Projectile-like fragment (PLF)) and fragment 2 (TLF), respectively. $C_{1,2}$ are the LDM stiffness parameters of the fragments [54]. d_{Z_1,N_1,β_2} is the microscopic dimension in the state (Z_1, N_1, β_2). $W_{Z_1,N_1,\beta_2;Z_1',N_1,\beta_2}$ is the mean transition probability from the state (Z_1, N_1, β_2) to (Z_1', N_1, β_2) [55].

The potential energy surface (U) can be calculated as [45,49]

$$\begin{aligned}
U(Z_1,N_1,\beta_2,J,R_{\rm cont}) &= \Delta(Z_1,N_1)+\Delta(Z_2,N_2)\\
&+V(Z_1,N_1,\beta_2,J,R_{\rm cont})+\frac{1}{2}C_1(\delta\beta_2^1)^2+\frac{1}{2}C_2(\delta\beta_2^2)^2.
\end{aligned} \tag{2}$$

The last two terms are dynamical deformation energies of the PLF and TLF. $\Delta(Z_i,N_i)$ $(i = 1, 2)$ is mass excess of the fragment i. The detailed description of $\Delta(Z_i,N_i)$ can be seen in Ref. [49].

The shell correction in U is estimated as [56]

$$E_{\rm sh}(Z_i,N_i) = E_{\rm sh}^0(Z_i,N_i)e^{-E^*/E_{\rm d}}. \tag{3}$$

$E_{\rm sh}^0$ is the shell correction energy on the ground state, which is prescribed by Strutinsky [57,58]. The damping parameter $E_{\rm d} = 5.48A_i^{1/3}/(1+1.3A_i^{-1/3})$ MeV.

The effective nucleus-nucleus interaction potential V can be written as

$$\begin{aligned}
V(Z_1,N_1,\beta_2,J,R_{\rm cont}) &= V_{\rm N}(Z_1,N_1,\beta_2,R_{\rm cont})\\
&+V_{\rm C}(Z_1,N_1,\beta_2,R_{\rm cont})+\frac{(J\hbar)^2}{2\zeta_{\rm rel}}.
\end{aligned} \tag{4}$$

The detailed description of nuclear potential $V_{\rm N}$ and Coulomb potential $V_{\rm C}$ can be seen in Ref. [49,59,60]. $\zeta_{\rm rel} = \mu(R_{\rm cont})^2$ is the moment of inertia for relative motion of the DNS. μ is the reduced mass of the DNS. In diffusion process (solving the master equation), the tip-tip orientation is usually considered for calculating the potential energy surface in the DNS model [23–25,61].

The production cross sections of the primary products in transfer reactions can be calculated as follows [61]:

$$\begin{aligned}
\sigma_{\rm pr}(Z_1,N_1) &= \frac{\pi\hbar^2}{2\mu E_{\rm c.m.}}\times\\
&\sum_{J=0}^{J_{\max}}(2J+1)[T_{\rm cap}(J)\sum_{\beta_2}P(Z_1,N_1,\beta_2,J,\tau_{\rm int}(J))].
\end{aligned} \tag{5}$$

The contact time $\tau_{\rm int}$ is determined by deflection function method [62,63]. $T_{\rm cap}$ is the capture probability. For the reactions with potential pockets, $T_{\rm cap}$ is calculated with Hill-Wheeler formula [64], with consideration of Coulomb barrier distribution. The Coulomb barrier distribution is related to the orientation effects of deformed system. On the other hand, for the heavy systems without potential pockets (there are no ordinary barriers: the potential energies of these nuclei are everywhere repulsive), $T_{\rm cap}$ is estimated as 1, when the incident energy is above the interaction potential at the contact configuration ($V_{\rm DF}$) [24,61]. Otherwise, if $E_{\rm c.m.} < V_{\rm DF}$, $T_{\rm cap} = 0$. For the deformed systems, $V_{\rm DF}$ is calculated in the tip-tip collisions. The contact position where the nucleon transfer process takes place for the heavy system without potential pocket can be obtained with the equation: $R_{\rm cont} = R_1(1+\beta_2^1Y_{20}(\theta_1)) + R_2(1+\beta_2^2Y_{20}(\theta_2)) + 0.7$ fm. Here, $R_{1,2} = 1.16A_{1,2}^{1/3}$ fm. For the prolate deformation, $\theta_{1,2} = 0$. $\beta_2^1 = \beta_2^{\rm p}+\delta\beta_2^1$ and $\beta_2^2 = \beta_2^{\rm t}+\delta\beta_2^2$ denote the quadrupole deformation of the PLF and TLF, respectively. Here, $\beta_2^{\rm p}$ and $\beta_2^{\rm t}$ denote the static quadrupole deformation of the projectile and target, respectively. For all reactions in this work, the potential energies are everywhere repulsive and there are no potential pockets.

The sharing of the excitation energy between the primary fragments was assumed to be proportional to their masses. The excitation energy of the primary fragment i formed at the entrance angular momentum J can be calculated as [65]

$$\begin{aligned}
E^*_{Z_i,N_i,J} &= \frac{\sum_{\beta_2}[P(Z_i,N_i,\beta_2,J,t=\tau_{\rm int})E^*_{\rm DNS}(Z_i,N_i,\beta_2,J,t=\tau_{\rm int})]}{\sum_{\beta_2}P(Z_i,N_i,\beta_2,J,t=\tau_{\rm int})}\\
&\times\frac{A_i}{A_{\rm tot}}.
\end{aligned} \tag{6}$$

A_i and $A_{\rm tot}$ are mass numbers of fragment i and whole system, respectively. $E^*_{\rm DNS}$ is the local excitation energy and can be written as

$$\begin{aligned}
E^*_{\rm DNS}(Z_1,N_1,\beta_2,J,t) =& E_{\rm diss}(J,t)-[U(Z_1,N_1,\beta_2,J,R_{\rm cont})\\
&-U(Z_{\rm p},N_{\rm p},\beta_2,J,R_{\rm cont})],
\end{aligned} \tag{7}$$

and

$$\begin{aligned}
E_{\rm diss}(J,t) =& E_{\rm c.m.}-V(Z_{\rm p},N_{\rm p},\beta_2=0,J=0,R_{\rm cont})\\
&-\frac{(J'(t)\hbar)^2}{2\zeta_{\rm rel}}-E_{\rm rad}(J,t).
\end{aligned} \tag{8}$$

Here, $J'(t)$ $(= J_{\rm st}+(J-J_{\rm st})e^{-t/\tau_J})$ is the angular momentum at time t. $J_{\rm st} = \frac{\zeta_{\rm rel}}{\zeta_{\rm tot}}J$. $\zeta_{\rm tot}(=\zeta_{\rm rel}+\zeta_{\rm int}^{\rm p}+\zeta_{\rm int}^{\rm t})$ is the total moment of inertia for the DNS. $\zeta_{\rm int}^{\rm p}$ and $\zeta_{\rm int}^{\rm t}$ are intrinsic moments of inertia [66] for the projectile and target, respectively. $E_{\rm rad}(J,t) = [E_{\rm c.m.}-$

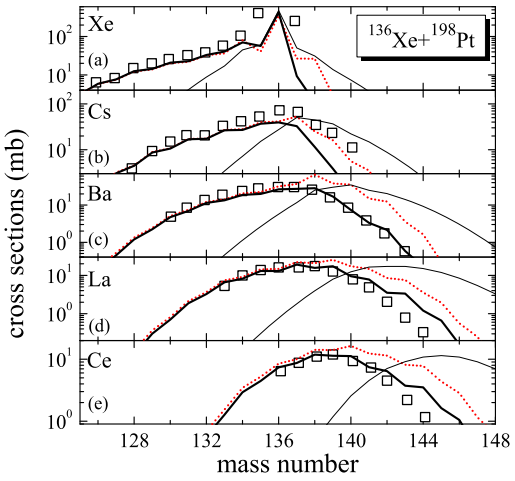

Fig. 1. Calculated cross sections in the proton pick-up channel in the reaction ^{136}Xe + ^{198}Pt at $E_{\mathrm{c.m.}} = 643$ MeV. The experimental data [12] is also shown with squares. The thick and thin solid lines denote the calculated cross sections of final products and primary fragments, respectively. The red dotted lines denote the calculated cross sections of final products without shell corrections.

$V(Z_{\mathrm{p}}, N_{\mathrm{p}}, \beta_2 = 0, J = 0, R_{\mathrm{cont}}) - \frac{(J\hbar)^2}{2\zeta_{\mathrm{rel}}}]e^{-t/\tau_R}$. τ_J $(= 12 \times 10^{-22}$ s) and τ_R $(= 2 \times 10^{-22}$ s) are respectively the characteristic relaxation time of angular momentum and radial energy.

In this work, the GEMINI++ code is applied to describe the deexcitation process [67]. The GEMINI++ code could give a good description of the spectral shape of evaporation spectra systematically [67] and unified description of fission in fusion and spallation [68]. The successful description of de-excitation process with the GEMINI++ code in the MNT reactions has been noticed in combination with the DNS model [69], TDHF approach [35,37] and GRAZING model [70]. Beside, based on the comparison with different models, it was noticed that the GEMINI++ was the most reliable code [71].

In Fig. 1, the calculated production cross sections of PLF produced in the reaction ^{136}Xe + ^{198}Pt from the proton pick-up channel, which is the pathway of producing the unknown $N = 126$ isotones, are compared with the experimental data [12]. It can be seen that the calculated results (denoted with thick solid lines) are in good agreement with the experimental data. It is worth to emphasize that parameters in the DNS model are fixed in the related works. The default parameter set of the GEMINI++ code is used. The thin solid lines denote the cross sections of primary product. One can see that several neutrons are evaporated in the de-excitation process. We also show the calculated cross sections of final products without shell corrections in the potential energy surface (denoted with red dotted lines). The inclusion of shell corrections strongly improves description of experimental data, which gives us a definite confidence for investigating the shell inhibition on production cross sections.

3. Results and discussion

In Fig. 2, we show the production cross sections of ^{200}W as a function of incident energy in the reactions ^{136}Xe + ^{198}Pt, ^{136}Xe + ^{208}Pb, ^{186}W + ^{238}U, and ^{208}Pb + ^{238}U. For each reaction, the cross section first increases strongly with the increasing incident energy. Then, the behavior of weak energy dependence is noticed after reaching a relatively high level of cross sections. This is because the main events are quasielastic collisions at low incident energy region. With increase of incident energy, the contact time of DNS increases, which enhances the contributions of DIC. Therefore, the cross sections of primary fragments contributing to the yields of ^{200}W will increase strongly. As the incident energy continues to

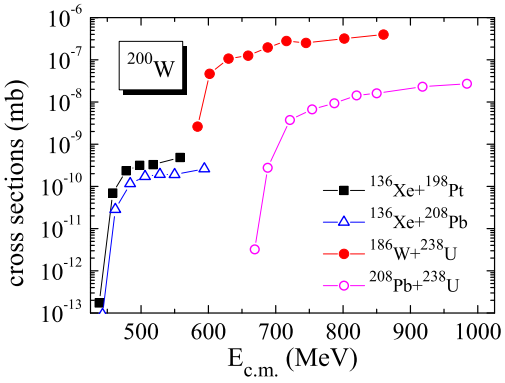

Fig. 2. Cross sections as a function of incident energy for producing unknown isotope ^{200}W in the MNT reactions ^{136}Xe + ^{198}Pt, ^{136}Xe + ^{208}Pb, ^{186}W + ^{238}U, and ^{208}Pb + ^{238}U.

increase, the suppressed evaporation probabilities counteract the enhanced cross sections of primary fragments, which gives rise to the saturation of cross section of final product. The similar behavior is also noticed based on a Langevin-type approach [33].

In comparison to the ^{136}Xe induced reactions, the ^{238}U target shows great advantages for producing ^{200}W. The effects of mass asymmetry relaxation [61,72], N/Z equilibration [19,20,73], and shell closures [45–49] play an important role in DIC. With investigation of these effects, the advantages of the ^{238}U target for producing NRI have been shown in Ref. [61]. Also, the unknown exotic isotopes could be observed from projectile-like products. Hence, we choose the combinations with ^{238}U target as candidates for producing NRI around $N = 126$. As well known, the incident energy plays an important role on successful observation of new NRI. Based on the results shown in Fig. 2, the optimal incident energies of 1.3 times interaction barrier (V_{DF}), which is calculated with double folding potential, in the entrance channel are estimated and studied in the following. $V_{\mathrm{DF}} = 399$, 422, 555, 573, 618, 637, and 656 MeV, respectively, for the reactions ^{136}Xe + ^{198}Pt, ^{136}Xe + ^{208}Pb, ^{182}Hf + ^{238}U, ^{186}W + ^{238}U, ^{198}Pt + ^{238}U, ^{204}Hg + ^{238}U, and ^{208}Pb + ^{238}U.

In Fig. 2, it can be seen that the production cross sections of ^{200}W in the reaction ^{186}W + ^{238}U are several orders of magnitude higher than those in the reaction ^{208}Pb + ^{238}U. In the combinations with ^{208}Pb, the protons are supposed to transfer from ^{208}Pb to another partner. By contrast, the ^{186}W pick-up neutrons in the collisions for producing ^{200}W. The N/Z ratio of ^{186}W is 1.51, which is close to 1.54 of ^{208}Pb. Hence, the effect of N/Z equilibration is weak. Is this phenomenon mainly due to the lower transfer probabilities of protons? Intriguingly, beyond expectation, the cross sections in the reactions ^{136}Xe + ^{198}Pt and ^{136}Xe + ^{208}Pb are close, although the number of stripping protons from ^{208}Pb is twice over that from ^{198}Pt. The yields of the final products not only depend on the cross sections of primary fragments, but also depend on the evaporation probabilities in the specific channels. Furthermore, the behaviors inspire us to make conjecture that the shell closures in the above combinations could remarkably suppress the production cross sections of ^{200}W. We will gain a deep insight into above behaviors in the following.

We show the ratio of cross sections for producing ^{200}W in the reaction ^{208}Pb + ^{238}U to those in the reaction ^{186}W + ^{238}U (denoted with $\sigma_{\mathrm{Pb\text{-}induced}}/\sigma_{\mathrm{W\text{-}induced}}$) in Fig. 3 (a). It is shown that with increasing incident energy the value of $\sigma_{\mathrm{Pb\text{-}induced}}/\sigma_{\mathrm{W\text{-}induced}}$ increases strongly and reaches the saturated value of 0.05. In order to clarify this behavior, the results without shell corrections are also shown. For the case of without shell corrections, the ratio of $\sigma_{\mathrm{Pb\text{-}induced}}/\sigma_{\mathrm{W\text{-}induced}}$ is strongly enhanced, especially for the incident energy around V_{DF}. With increase of incident energy, the shell

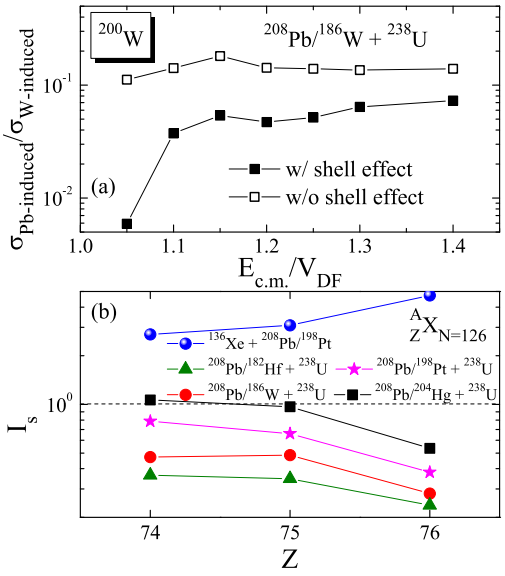

Fig. 3. (a) Ratios of production cross sections of ^{200}W in the reaction ^{208}Pb + ^{238}U to those in the reaction ^{186}W + ^{238}U ($\sigma_{\text{Pb-induced}}/\sigma_{\text{W-induced}}$) as a function of incident energy. The open squares show the results without shell effects. (b) Relative shell inhibition factor I_s for producing unknown $N = 126$ isotones ^{200}W, ^{201}Re, and ^{202}Os in different combination pairs at $E_{\text{c.m.}} = 1.3 \times V_{\text{DF}}$.

effects are weakened because of the high temperature of the DNS system during the evolution. Therefore, the shell inhibition plays a significant role for producing $N = 126$ isotones in the ^{208}Pb induced reaction, especially with incident energy around V_{DF}.

To investigate the relative shell inhibition effect in the MNT reactions for producing NRI around $N = 126$ and provide a guidance for selecting the favorable combinations, we define a relative shell inhibition factor I_s, which can be written as

$$I_s = \frac{(\sigma_X/\sigma_Y)_{\text{with-shell}}}{(\sigma_X/\sigma_Y)_{\text{without-shell}}}. \tag{9}$$

I_s denotes the relative shell inhibition magnitude between the reactions X and Y. In Fig. 3 (b), we show the values of I_s for several combination pairs. It is noticed that the factor I_s could sensitively present the shell discrepancies in different reactions. The incident energy of $E_{\text{c.m.}} = 1.3 \times V_{\text{DF}}$ is used for each reaction. It can be seen that the values of I_s for producing ^{200}W, ^{201}Re, and ^{202}Os are lower than 1 for the combination pairs ^{208}Pb/^{182}Hf + ^{238}U, ^{208}Pb/^{186}W + ^{238}U, and ^{208}Pb/^{198}Pt + ^{238}U. It means that the shell inhibition effect is much stronger in the reaction ^{208}Pb + ^{238}U in comparison to the ^{182}Hf, ^{186}W, and ^{198}Pt induced ones. Also, from ^{182}Hf to ^{208}Pb, the neutron and proton numbers get closer to the shell closures $Z = 82$ and $N = 126$, which results in stronger shell effects and enhancement of I_s values closer to 1. Interestingly, the I_s values for the reactions ^{136}Xe + ^{208}Pb/^{198}Pt are larger than 1, which means the reaction ^{136}Xe + ^{198}Pt shows stronger shell inhibition than the reaction ^{136}Xe + ^{208}Pb for producing ^{200}W, ^{201}Re, and ^{202}Os. The reasons for this phenomenon are as follows. (i) There is neutron shell closure $N = 82$ for the projectile ^{136}Xe. For producing ^{200}W, ^{201}Re, and ^{202}Os in the reaction ^{136}Xe + ^{198}Pt, the main pathway is neutron transfer. The neutron shell closure $N = 82$ also inhibits the neutron transfer and suppresses the yields of exotic nuclei. (ii) The proton and neutron numbers of ^{198}Pt are close to the shell closures of $Z = 82$ and $N = 126$. The effects of shell closures still exist. Therefore, the conjecture made in Fig. 2 is testified. Overall, from the factor I_s, the strong shell inhibition for the reactions involving ^{208}Pb is clearly shown.

To further clarify the shell inhibition effect and inferiority of cross sections in ^{208}Pb induced reactions, we show the yield contributions in xn evaporation channels for producing ^{200}W in the reactions ^{186}W + ^{238}U (745 MeV) and ^{208}Pb + ^{238}U (850 MeV) in Fig. 4 (b). The main evaporation channel (2n) is denoted with vertical dashed line, which bridges the final yields contribution for producing ^{200}W with the corresponding yields of the primary fragments shown in Fig. 4 (a). One can see that the yield contribution in the 2n channel for the reaction ^{208}Pb + ^{238}U is about two orders of magnitude lower than that for the reaction ^{186}W + ^{238}U. However, the cross sections of the primary fragments ^{202}W* are close. Therefore, the discrepancy of yields in two reactions mainly results from evaporation process. Fig. 4 (c) shows the yields of primary fragments ^{202}W* and ^{204}W* as a function of $E_{\text{c.m.}}/V_{\text{DF}}$ in the reactions ^{186}W + ^{238}U and ^{208}Pb + ^{238}U. It is found that the advantages of the reaction ^{186}W + ^{238}U are weakened with increasing incident energy. This is because the inferiority of probability for

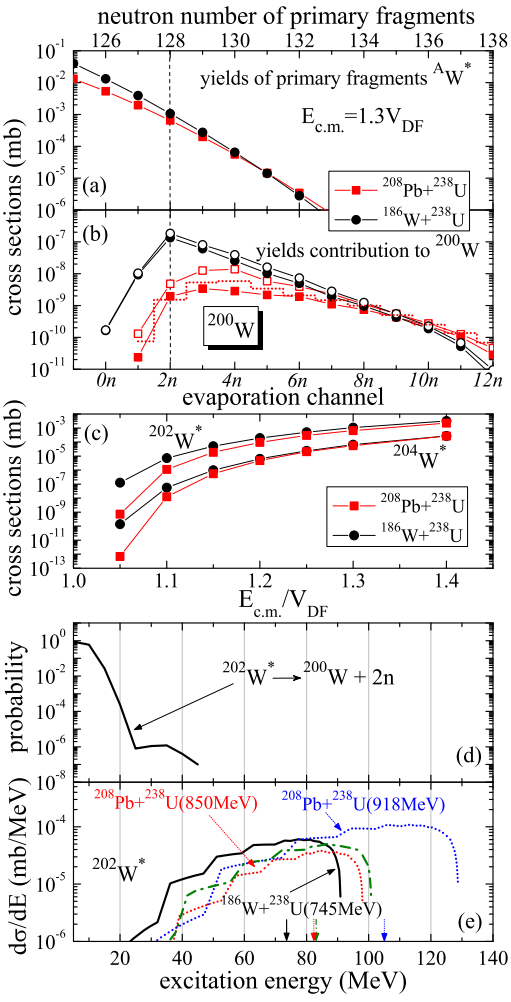

Fig. 4. (a) Yields of primary fragments ^{A}W* produced in the reactions ^{186}W + ^{238}U (745 MeV) and ^{208}Pb + ^{238}U (850 MeV). (b) Contributions of cross sections from the primary Tungsten fragments for producing ^{200}W in xn evaporation channels in the reactions ^{186}W + ^{238}U (745 MeV) and ^{208}Pb + ^{238}U (850 MeV). The results without shell corrections are denoted with open circles and squares in the reactions ^{186}W + ^{238}U (745 MeV) and ^{208}Pb + ^{238}U (850 MeV), respectively. The dotted lines indicate the results at $E_{\text{c.m.}} = 918$ MeV for ^{208}Pb + ^{238}U. (c) The incident energy dependence of yields of primary fragments ^{202}W* and ^{204}W* produced in the reactions ^{186}W + ^{238}U and ^{208}Pb + ^{238}U. (d) Probabilities of evaporation channels ^{202}W* → ^{200}W+2n as a function of excitation energy, calculated within GEMINI++ code. The spin angular momentum is set to 0. (e) The excitation energy distributions for the primary fragments ^{202}W* formed in the reactions ^{208}Pb + ^{238}U and ^{186}W + ^{238}U. The olive dash-dotted line denotes the result in the reaction ^{208}Pb + ^{238}U (850 MeV) without shell corrections. The vertical arrows denote the average values of the excitation energies.

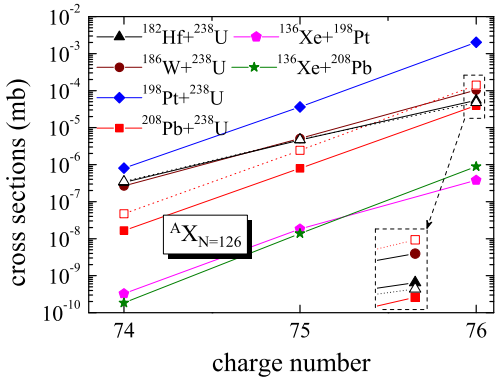

Fig. 5. Predicted production cross sections of ^{200}W, ^{201}Re, and ^{202}Os in the reactions ^{182}Hf, ^{186}W, ^{198}Pt, ^{208}Pb + ^{238}U, ^{136}Xe + ^{208}Pb, and ^{136}Xe + ^{198}Pt. The open triangles and open squares denote the results without shell effects in the reactions ^{182}Hf + ^{238}U and ^{208}Pb + ^{238}U, respectively. $E_{\mathrm{c.m.}} = 1.3 \times V_{\mathrm{DF}}$.

proton transfer (due to Coulomb barrier inhibition) in comparison to neutron transfer is reduced with increasing incident energy.

Furthermore, if the shell corrections in the PES are removed, the strong enhancement of yield for the reaction ^{208}Pb + ^{238}U can be seen in Fig. 4 (b) and only slight increase of yields is shown for the reaction ^{186}W + ^{238}U. As shown in Fig. 4 (a), the production cross section of the primary fragments ^{202}W* in the reactions ^{208}Pb + ^{238}U is 0.7 μb, which is a little lower than 0.9 μb of the case without shell corrections. Hence, the shell effects not only influence the probability of the nucleon transfer, but also play an important role in the second stage of reaction (de-excitation process) with influence of the excitation energy distribution of the primary fragments. In Fig. 4 (b), we also show the result in the reaction ^{208}Pb + ^{238}U at $E_{\mathrm{c.m.}} = 918$ MeV with red dotted line. Interestingly, the behavior of weak energy dependence is displayed in each single evaporation channel.

To explain the above phenomena, we show the probability of evaporation channel ^{202}W* $\rightarrow$ ^{200}W + 2n as a function of excitation energy in Fig. 4 (d). It can be seen that the probability decreases strongly with increasing excitation energy. Correspondingly, the excitation energy distributions for the fragments ^{202}W* are displayed in Fig. 4 (e). The average value of excitation energy for the ^{202}W* fragments in the reaction ^{186}W + ^{238}U (745 MeV) is 73.8 MeV, which is lower than 82.3 MeV produced in the reaction ^{208}Pb + ^{238}U (850 MeV). The excitation energy distribution for ^{202}W* produced in the reaction ^{186}W + ^{238}U locates at the relatively low energy region, which corresponds to the higher evaporation probability. This is because the production of ^{202}W* is associated with a lot of protons transfer and large amount of energy dissipation in the reaction ^{208}Pb + ^{238}U. The olive dash-dotted line denotes the result without shell corrections for the reaction ^{208}Pb + ^{238}U (850 MeV). Although the total cross sections of ^{202}W* are close, the advantage of ^{202}W* yields for the case without shell effects in low excitation energy region strongly enhances the final yield of ^{200}W. The excitation energy distribution in ^{208}Pb + ^{238}U at $E_{\mathrm{c.m.}} = 918$ MeV is also presented. The increase of incident energy enhances the total cross section of primary ^{202}W* fragment. However, the extra yields are highly excited, which corresponds to the very low survival probability through the channel of 2n evaporation. Consequently, the cross section contribution to ^{200}W from the extra yields of ^{202}W* would be negligible, which successfully accounts for the behavior of weak energy dependence, as shown in Fig. 2, Fig. 4 (b), and in Refs. [33,26].

Fig. 5 shows the comparison of the cross sections for producing ^{200}W, ^{201}Re, and ^{202}Os among several MNT reactions based on the ^{238}U target. The inferiority of cross section can be clearly seen in the reaction ^{208}Pb + ^{238}U. The production cross section of ^{202}Os in the reaction ^{208}Pb + ^{238}U is 39 nb, which is lower than 55 nb in the reactions ^{182}Hf + ^{238}U. We also present the results without shell effects in the reactions ^{208}Pb + ^{238}U and ^{182}Hf + ^{238}U. For producing ^{202}Os, the reversal of cross section is clearly shown. As shown in 3 (b), in comparison to the reaction ^{182}Hf + ^{238}U, the shell inhibition in the reaction ^{208}Pb + ^{238}U is strong ($I_s = 0.24$ for ^{202}Os), which results into unfavorable property for producing ^{202}Os in ^{208}Pb induced reaction. The results in the reactions ^{136}Xe + ^{198}Pt and ^{136}Xe + ^{208}Pb are also shown. The yields are at least 2 orders of magnitude lower than the reactions based on the ^{238}U target. The beam intensities for ^{136}Xe and ^{208}Pb at GSI reach 10^{10} and 0.5×10^{10} p/s, respectively. The values of factor "cross section $\times$ beam intensity" for producing ^{202}Os, ^{201}Re, and ^{200}W in the reaction ^{136}Xe + ^{198}Pt are 3.8×10^3, 184, and 3.2 mb·p/s, respectively, which is much lower than 1.5×10^5, 4×10^3, and 80 mb·p/s in the reaction ^{208}Pb + ^{238}U. Therefore, from the relative comparisons, it is shown that the reactions ^{136}Xe + ^{198}Pt and ^{136}Xe + ^{208}Pb are not the good candidates for producing unknown $N = 126$ isotones.

4. Summary

In summary, it is necessary to explore the optimal conditions for producing $N = 126$ isotones. The relative shell inhibition on production yields of $N = 126$ isotones is investigated within the DNS-sysu model in combination with the GEMINI++ code. For the first time, with definition of the relative shell inhibition factor, we quantitatively evaluate and compare the shell effects on production yield of the $N = 126$ isotones between different combinations, which provides a perspective for selecting the optimal reactions. The reactions ^{208}Pb + ^{238}U and ^{186}W + ^{238}U for producing ^{200}W, in which the pathways of proton and neutron transfer are characterized respectively, in main evaporation channels are studied. It is found that the effect of shell inhibition is mainly related to the excitation energy distribution of the primary fragments and the corresponding neutron evaporation probabilities. Also, the weak energy dependence of cross sections for producing NRI around $N = 126$, which have been noticed in many works, is revealed with relevance between evaporation probabilities and excitation energy distributions of primary fragments. The results in this work suggest that the combinations with double closed shell structure, such as ^{208}Pb are unfavorable for producing unknown NRI. It is also demonstrated that the reactions ^{136}Xe + ^{198}Pt and ^{136}Xe + ^{208}Pb are not the good candidates.

Declaration of competing interest

The authors declare that they have no known competing financial interests or personal relationships that could have appeared to influence the work reported in this paper.

Acknowledgements

The author would like to acknowledge Professor R.J. Charity for valuable information about the GEMINI++ code, Dr. H.M. Devaraja for the valuable information of beam intensities at GSI, and Professor F.S. Zhang, Professor H.F. Zhang, Dr. P.W. Wen, Dr. C. Li, Dr. J. Su, Dr. X.J. Bao for fruitful discussions. This work was supported by the National Natural Science Foundation of China under Grants No. 12075327, No. 11605296, and No. 11875329.

References

[1] H. Grawe, L. Langanke, G. Martínez-Pinedo, Rep. Prog. Phys. 70 (2007) 1525.
[2] O. Sorlin, M.G. Porquet, Prog. Part. Nucl. Phys. 61 (2008) 602.
[3] M. Thoennessen, Discovery of nuclides project, https://people.nscl.msu.edu/~thoennes/isotopes/.

[4] T. Kurtukian-Nieto, J. Benlliure, K.H. Schmidt, et al., Phys. Rev. C 89 (2014) 024616.
[5] T. Ohnishi, T. Kubo, K. Kusaka, A. Yoshida, K. Yoshida, et al., J. Phys. Sci. Jpn. 79 (2010) 073201.
[6] V.V. Volkov, Phys. Rep. 44 (1978) 93.
[7] L. Corradi, G. Pollarolo, S. Szilner, J. Phys. G, Nucl. Part. Phys. 36 (2009) 113101.
[8] W. Loveland, Front. Phys. 7 (2019) 23.
[9] G.G. Adamian, N.V. Antonenko, A. Diaz-Torres, S. Heinz, Eur. Phys. J. A 56 (2020) 47.
[10] L. Zhu, C. Li, C.C. Guo, J. Su, P.W. Wen, G. Zhang, F.S. Zhang, Int. J. Mod. Phys. E 29 (2020) 2030004.
[11] F.S. Zhang, C. Li, L. Zhu, P.W. Wen, Front. Phys. 13 (2018) 132113.
[12] Y.X. Watanabe, Y.H. Kim, S.C. Jeong, et al., Phys. Rev. Lett. 115 (2015) 172503.
[13] V.V. Desai, W. Loveland, R. Yanez, G. Lane, S. Zhu, et al., Eur. Phys. J. A 56 (2020) 150.
[14] H.M. Devaraja, S. Heinz, D. Ackermann, et al., Eur. Phys. J. A 56 (2020) 224.
[15] J.S. Barrett, W. Loveland, R. Yanez, S. Zhu, et al., Phys. Rev. C 91 (2015) 064615.
[16] E.M. Kozulin, E. Vardaci, G.N. Knyazheva, et al., Phys. Rev. C 86 (2012) 044611.
[17] M.V. Pajtler, S. Szilner, et al., Nucl. Phys. A 941 (2015) 273.
[18] O. Beliuskina, S. Heinz, V. Zagrebaev, et al., Eur. Phys. J. A 50 (2014) 161.
[19] W. Królas, R. Broda, B. Fornal, T. Pawłat, et al., Nucl. Phys. A 724 (2003) 289–312.
[20] W. Królas, R. Broda, B. Fornal, T. Pawłat, et al., Nucl. Phys. A 832 (2010) 170–197.
[21] S. Heinz, O. Beliuskina, J. Phys. Conf. Ser. 515 (2014) 012007.
[22] G.G. Adamian, N.V. Antonenko, D. Lacroix, Phys. Rev. C 82 (2010) 064611.
[23] L. Zhu, J. Su, W.J. Xie, F.S. Zhang, Phys. Lett. B 767 (2017) 437.
[24] Yu.E. Penionzhkevich, G.G. Adamian, N.V. Antonenko, Phys. Lett. B 621 (2005) 119.
[25] X.J. Bao, Phys. Rev. C 102 (2020) 054613.
[26] Z.Q. Feng, Phys. Rev. C 95 (2017) 024615.
[27] M.H. Mun, K. Kwak, G.G. Adamian, N.V. Antonenko, Phys. Rev. C 101 (2020) 044602.
[28] P.W. Wen, A.K. Nasirov, C.J. Lin, H.M. Jia, J. Phys. G, Nucl. Part. Phys. 47 (2020) 075106.
[29] C. Li, F. Zhang, J. Li, L. Zhu, J. Tian, N. Wang, F.S. Zhang, Phys. Rev. C 93 (2016) 014618.
[30] C. Li, J. Tian, F.S. Zhang, Phys. Lett. B 809 (2020) 135697.
[31] K. Zhao, Z. Liu, F.S. Zhang, N. Wang, Phys. Lett. B 815 (2021) 136101.
[32] V.I. Zagrebaev, W. Greiner, Phys. Rev. C 83 (2011) 044618.
[33] A.V. Karpov, V.V. Saiko, Phys. Rev. C 96 (2017) 024618.
[34] S. Ayik, O. Yilmaz, B. Yilmaz, A.S. Umar, Phys. Rev. C 100 (2019) 044614.
[35] K. Sekizawa, S. Ayik, Phys. Rev. C 102 (2020) 014620.
[36] K. Sekizawa, Front. Phys. 7 (2019) 00020.
[37] X. Jiang, N. Wang, Phys. Rev. C 101 (2020) 014604.
[38] Z. Wu, L. Guo, Phys. Rev. C 100 (2019) 014612.
[39] A. Winther, Nucl. Phys. A 572 (1994) 191.
[40] R. Yanez, W. Loveland, Phys. Rev. C 91 (2015) 044608.
[41] P.W. Wen, C. Li, L. Zhu, C. Lin, F.S. Zhang, J. Phys. G, Nucl. Part. Phys. 44 (2017) 115101.
[42] Y.X. Watanabe, Y. Hirayama, N. Imai, H. Ishiyama, et al., Nucl. Instrum. Methods Phys. Res. B 317 (2013) 752–755.
[43] L. Corradi, S. Szilner, G. Pollarolo, D. Montanari, et al., Nucl. Instrum. Methods Phys. Res. B 317 (2013) 743–751.
[44] V.F. Comas, S. Heinz, S. Hofmann, et al., Eur. Phys. J. A 49 (2013) 112.
[45] V.I. Zagrebaev, W. Greiner, J. Phys. G, Nucl. Part. Phys. 34 (2007) 2265.
[46] E.M. Kozulin, G.N. Knyazheva, S.N. Dmitriev, I.M. Itkis, et al., Phys. Rev. C 89 (2014) 014614.
[47] W. Mayer, G. Beier, J. Friese, W. Henning, et al., Phys. Lett. B 152 (1985) 162.
[48] E.M. Kozulin, V.I. Zagrebaev, G.N. Knyazheva, I.M. Itkis, et al., Phys. Rev. C 96 (2017) 064621.
[49] L. Zhu, P.W. Wen, C.J. Lin, X.J. Bao, J. Su, C. Li, C.C. Guo, Phys. Rev. C 97 (2018) 044614.
[50] P.K. Sahu, A. Saxena, R.K. Choudhury, B.K. Nayak, D.C. Biswas, et al., Phys. Rev. C 68 (2003) 054612.
[51] V. Zagrebaev, W. Greiner, Phys. Rev. Lett. 101 (2008) 122701.
[52] T. Tanabe, R. Bock, M. Dakowski, A. Gobbi, H. Sann, H. Stelzer, U. Lynen, A. Olmi, D. Pelte, Nucl. Phys. A 342 (1980) 194.
[53] W. Nörenberg, Z. Phys. A 274 (1975) 241.
[54] W.D. Myers, W.J. Swiatecki, Nucl. Phys. 81 (1966) 1.
[55] S. Ayik, B. Schürmann, W. Nörenberg, Z. Phys. A 277 (1976) 299–310.
[56] A.V. Ignatyuk, M.G. Itkis, V.N. Okolovich, G.N. Smirenkin, A.S. Tishin, JETP Lett. 21 (1975) 74.
[57] P. Möller, J.R. Nix, W.D. Myers, W.J. Swiatecki, At. Data Nucl. Data Tables 59 (1995) 185.
[58] V.M. Strutinsky, Nucl. Phys. A 95 (1967) 420.
[59] G.G. Adamian, N.V. Antonenko, R.V. Jolos, S.P. Ivanova, O.I. Melnikova, Int. J. Mod. Phys. E 5 (1996) 191–216.
[60] C.Y. Wong, Phys. Rev. Lett. 31 (1973) 766.
[61] L. Zhu, C. Li, J. Su, C.C. Guo, W. Hua, Phys. Lett. B 791 (2019) 20–25.
[62] J.Q. Li, G. Wolschin, Phys. Rev. C 27 (1983) 590.
[63] G. Wolschin, W. Nörenberg, Z. Phys. A 284 (1978) 209–216.
[64] D.L. Hill, J.A. Wheeler, Phys. Rev. 89 (1953) 1102.
[65] L. Zhu, J. Phys. G, Nucl. Part. Phys. 47 (2020) 065107.
[66] A. Nasirov, A. Fukushima, Y. Toyoshima, Y. Aritomo, A. Muminov, S. Kalandarov, R. Utamuratov, Nucl. Phys. A 759 (2005) 342–369.
[67] R.J. Charity, Phys. Rev. C 82 (2010) 014610.
[68] D. Mancusi, R.J. Charity, J. Cugnon, Phys. Rev. C 82 (2010) 044610.
[69] G. Zhang, C.A.T. Sokhna, Z. Liu, F.S. Zhang, Phys. Rev. C 100 (2019) 024613.
[70] P.W. Wen, C.J. Lin, C. Li, L. Zhu, F. Zhang, F.S. Zhang, et al., Phys. Rev. C 99 (2019) 034606.
[71] B. Blanka, G. Canchela, F. Seisa, P. Delahaye, Nucl. Instrum. Methods B 416 (2018) 41–49.
[72] C. Simenel, K. Godbey, A.S. Umar, Phys. Rev. Lett. 124 (2020) 212504.
[73] Y. Iwata, T. Otsuka, J.A. Maruhn, N. Itagaki, Phys. Rev. Lett. 104 (2010) 252501.